Front. Struct. Civ. Eng. 2022, 16(6): 762–780
https://doi.org/10.1007/s11709-022-0847-8

RESEARCH ARTICLE

Analysis on damage causes of built-in corridor in core rock-fill dam on thick overburden: A case study

Jia'ao YU[a*], Zhenzhong SHEN[a,b], Zhangxin HUANG[a]

[a] *College of Water Conservancy and Hydropower Engineering, Hohai University, Nanjing 210024, China*
[b] *State Key Laboratory of Hydrology-Water Resources and Hydraulic Engineering, Hohai University, Nanjing 210024, China*
[*] *Corresponding author. E-mail: jiaaoyu@hhu.edu.cn*

ABSTRACT The stress state of the built-in corridor in core rock-fill dam on thick overburden is extremely complex, which may produce cracking and damage. The purpose of this paper was to investigate the effect of thick overburden on the stress and deformation of the built-in corridor in a rock-fill dam, and ascertain the damage causes of the corridor. The rationality of the analysis method for corridor with similar structure is another focus. The approach is based on finite-element method and the calculation result accuracy is verified by the field monitoring data. The improved analysis method for corridors with similar structure is proposed by comparing various corridor load calculation methods and concrete constitutive models. Results demonstrate that the damage causes of the corridor are the deformability difference between the overburden and concrete and the special structural form. And the calculation model considering dam construction process, contact between concrete and surrounding soil, and concrete damage plasticity can reasonably reflect the mechanical behavior of the corridor. The research conclusions may have a reference significance for the analysis of tunnels similar to built-in corridors.

KEYWORDS thick overburden, built-in corridor, stress, deformation, causes for damage, concrete damaged plasticity

1 Introduction

Thick overburden refers to loose deposits with a thickness of more than 30 m accumulated on the riverbed [1], which is widely distributed in river valleys in southwest China. In the construction of water conservancy projects, the method of full excavation of thick overburden is rarely utilized to clear the foundation due to the huge amount of work and economic infeasibility. With the advantage of strong adaptability to foundation deformation, the earth rock dam can be directly built on thick overburden.

On this condition, seepage prevention is the crux for the normal operation of earth rock dams. Generally, the anti-seepage system of high earth rock dams is composed of core wall, cement grouting, concrete cut-off wall and their connection part [2,3]. The amount of grouting for the cut-off wall of earth rock dam on thick overburden is large. In order to facilitate the construction, generally the grouting corridor is fixed on the top of the cut-off wall to connect the cut-off wall with the core wall. In this case, the corridor is deeply buried in the dam body, with its bottom connected with the cut-off wall. Therefore, the stress and deformation of the corridor is very complicated, and corridor cracking has occurred in many built projects [4–7]. It is of great significance to correctly analyze the cracking causes of the built-in corridor and put forward a reasonable numerical method for corridor structure.

At present, the design of section shape and lining thickness of foundation grouting corridor of earth rock dam is still carried out by finite element method based on the calculation of the surrounding pressure for tunnels. Thus, the determination of the distribution law of surrounding pressure is the most crucial basis. The calculation of surrounding pressure abroad is mainly established by theoretical analysis, which started earlier and is relatively perfect [8–10]. For example, Terzaghi formula and Bierbaumer formula comprehensively consider the influence of buried depth, height and span of

Article history: Received Jan 9, 2022; Accepted Mar 23, 2022

corridor, internal friction angle and cohesion of surrounding rock [11,12].

The design of built-in corridor in earth rock dam in China mostly refers to the relevant design specifications for tunnels, and the calculation of surrounding pressure is mainly based on empirical formulas [13–15]. For example, the specification for design of hydraulic tunnel (SL279-2012) points out that the support and lining design for tunnels shall fully consider the self-stability and bearing capacity of the surrounding rock [14]. The surrounding pressure is calculated only by considering the height and span of tunnels, and the influence of surrounding rock mechanical properties and other factors are not taken into account. It can be seen that the factors considered and the scope of application of calculation formulas for surrounding rock pressure are different, and these formulas may be not very reasonable in some specific cases.

On the other hand, because the lining material of corridors is usually reinforced concrete, it is generally simulated by linear elastic model. However, the relationship between stress and strain of the built-in corridor in earth rock dam after cracking no longer follows linearity [16]. Thus, the effect of concrete plasticity on the deformation of built-in corridor is necessary to be considered. Many researchers have used various concrete constitutive models to analyze the damage and cracking behavior of tunnels in recent years [17–24].

To sum up, the built-in corridor in actual earth rock dam engineering is usually designed by the combination of concrete linear elastic constitutive model and load calculation formula at present. However, several corridors designed by this method have cracked, which illustrates that the rationality of corridor structure analysis based on traditional surrounding pressure calculation and linear elastic model is difficult to be guaranteed. Using a core rock-fill dam with a built-in grouting corridor on thick overburden in southwest China as the studied case, the cracking and damage of built-in corridor is numerically analyzed by finite element method in this paper. In order to reasonably analyze the damage causes of the built-in corridor and improve the design method for corridors with similar structure, a more comprehensive static analysis finite element model and concrete constitutive model are adopted in this paper, and the results are compared with those obtained by traditional methods. By researching the deformation and stress development of corridor during dam construction and reservoir storage, this paper explicates the main causes of corridor damage. Besides, by comparing various calculation methods of surrounding pressure and concrete constitutive models, a reasonable model for structural analysis of the built-in corridor is put forward. The research conclusion has extensive reference significance for the design of tunnels in similar projects in the future.

2 Description of the studied case

2.1 Project overview

A hydropower station completed in 2012 is located in southwest China. The average annual flow at damsite is 29.5 m^3/s, and the reservoir capacity is 1.327×10^8 m^3 at the normal storage level of 2540.00 m. The engineering grade is second class large (2) type. The main water retaining structure of the hydropower station is a gravelly soil core rock-fill dam, with a crest elevation of 2544.00 m, a crest width of 12.00 m and a total crest length of 310.14 m. The maximum thickness of the dam foundation overburden is about 100 m. As a result, a 1.2 m-thick concrete cut-off wall was constructed inside the overburden. Meanwhile, the cut-off wall connects with the core wall through a built-in corridor, and embeds into the bedrock for a certain distance to ensure the formation of a complete vertical anti-seepage system. Figure 1 shows the typical cross-section of the core rock-fill dam.

In the initial design scheme, the built-in corridor is in city-gate shaped cross-section, with a clearance size of 3.5 m × 4.0 m. Besides, the top elevation of corridor baseplate is 2410.50 m, and the thickness of side wall, vault and baseplate is respectively 1.0, 1.0, and 3.65 m. After being damaged by the earthquake in 2008, the corridor was further reinforced by adding a new layer of concrete lining. The structure of the built-in corridor is illustrated in Fig. 2.

2.2 Safety inspection

2.2.1 Dam deformation monitoring

Currently, the dam of hydropower station has been in operation for almost ten years. Therefore, several serious safety problems have occurred, such as severe seepage, settlement exceeding the expected value and built-in corridor cracking. Hence, the safety inspection of the dam is arranged.

According to the dam safety monitoring results, the dam settlement along the river is small in the middle and large on both upstream and downstream sides, and the maximum settlement of the dam crest is 1204.2 mm. In the horizontal direction, the dam body presents deformation towards downstream, the higher the elevation, the greater the deformation, and the maximum horizontal displacement is 746 mm. The settlement and horizontal deformation distribution of the typical section are shown in Fig. 3.

2.2.2 Corridor deformation and cracking

In terms of corridor deformation, based on the safety inspection, the downstream surface of the side wall and

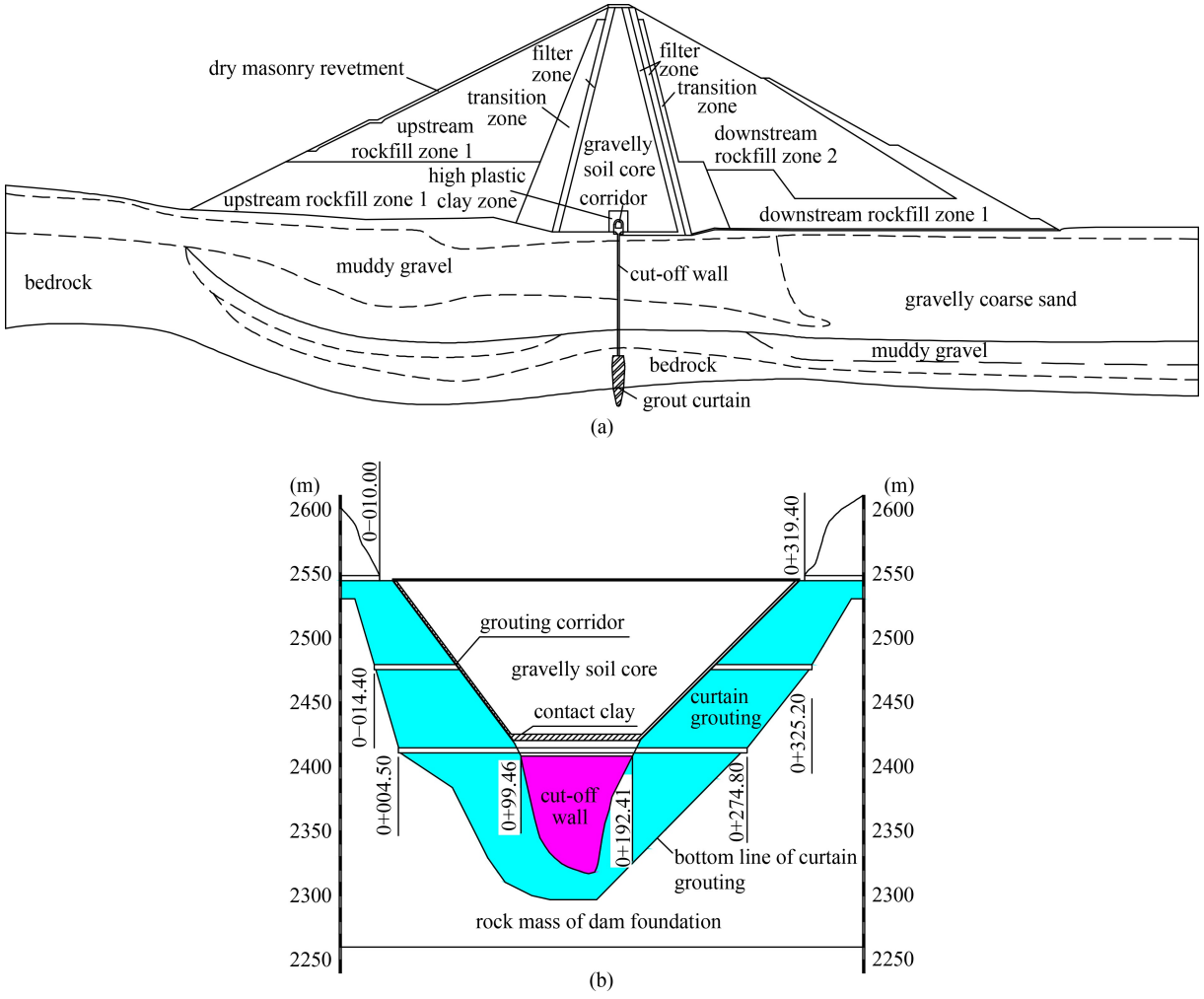

Fig. 1 Typical cross-section of the core rock-fill dam. (a) 0+150 m cross-section; (b) cross-section at the dam axis.

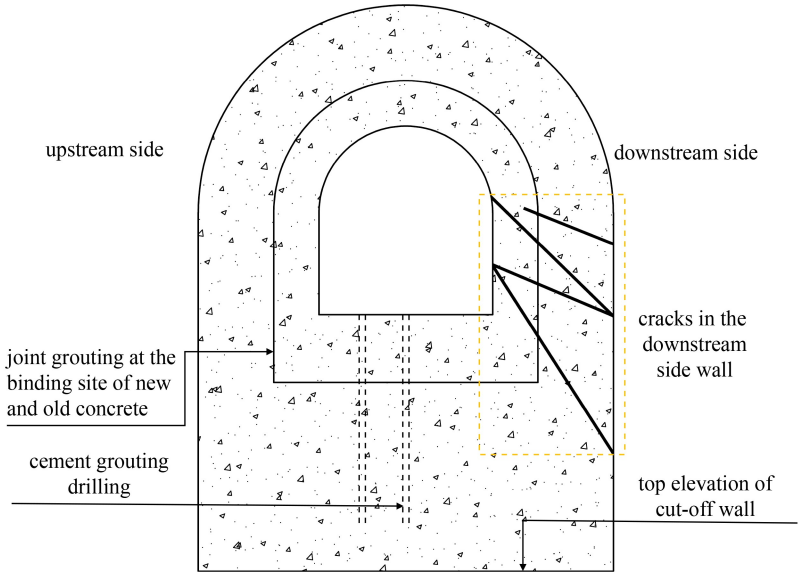

Fig. 2 Current situation of foundation grouting corridor.

its junction with the vault appears swelling phenomenon. At the lower part of the downstream, wall cracks present pressure-shear condition, and water seeps from these cracks, as shown in Fig. 4. In the subsequent regular

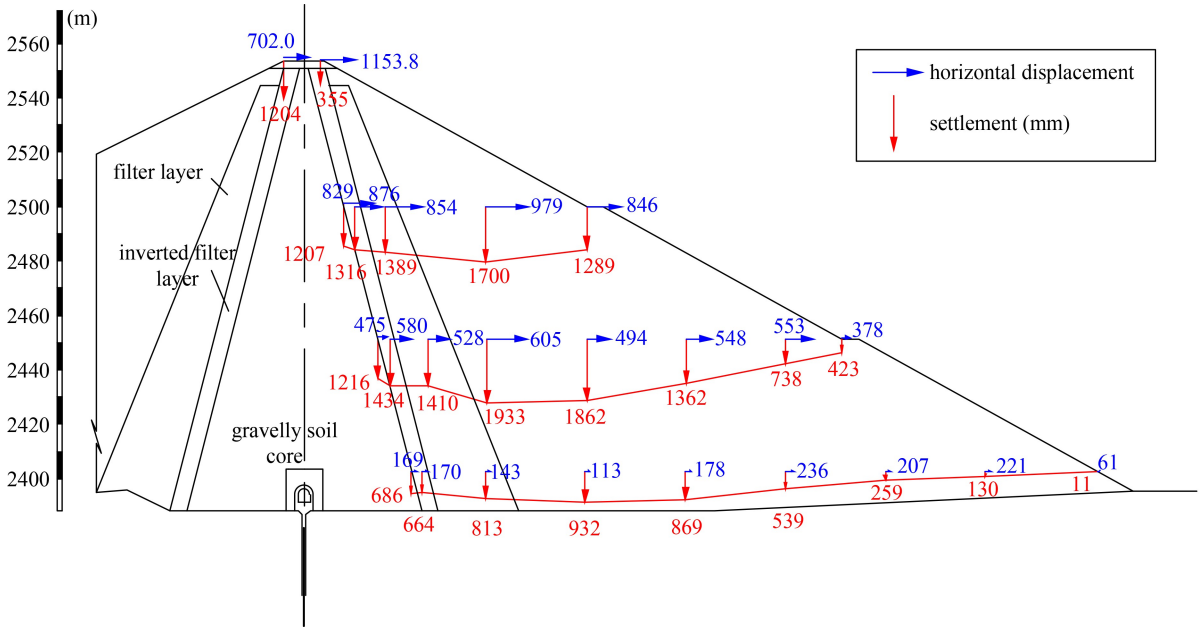

Fig. 3 Settlement and horizontal deformation distribution of the typical section.

inspections, it is found that the flow of water seepage, the width of cracks has a gradual increasing tendency. At present, the width of the crack is about 3–17 mm and the depth is about 60–80 cm. The current situation of cracks is shown in Fig. 2.

The corridor cracking along the dam axis is shown in Fig. 5. It can be seen from the figure that the cracking orientation of the built-in corridor is basically parallel to the dam axis and concentrated at the downstream side wall. Therefore, the section of the dam body in the middle of the riverbed is cut to establish a quasi-three-dimensional local model to analyze the causes of cracks, and the analyze results are able to represent the actual causes of corridor damage.

3 Corridor structure analysis based on surrounding pressure calculation

3.1 Calculation method of surrounding pressure

The Terzaghi formula and the specification for design of hydraulic tunnel (SL279-2002) are used to calculate the surrounding rock pressure in this paper. The Terzaghi formula comprehensively considers the cohesion strength of surrounding rock (soil), friction angle and geometric size of corridor, which is as follows [13]:

$$q_t = \frac{a_1(\gamma_R - c/a_1)}{K\tan\varphi}\left(1 - e^{-KH\tan\varphi/a_1}\right), \tag{1}$$

with

$$a_1 = \frac{b}{2} + h\tan\left(45^\circ - \frac{\varphi}{2}\right), \tag{2}$$

(a) (b)

Fig. 4 Deformation and cracking of corridor. (a) Deformation of corridor; (b) cracks and seepage at the downstream wall.

where b and h are respectively the excavation width and height of corridor, H is the buried depth of corridor, K is the horizontal coefficient of lateral earth pressure, c and φ are the friction angle and cohesion strength of surrounding rock (soil), respectively, γ_R is the bulk density of surrounding rocks and soils.

Based on the specification for design of hydraulic tunnel (SL279-2012), the loads exerted on the lining of the built-in corridor in an earth rock dam include self-weight, surrounding pressure, external water pressure, etc. The corridor is deeply buried at the bottom of the core rock-fill dam, and the overlying surrounding soil is loose. In this case, the value of surrounding pressure can be appropriately reduced [14]. The vertical and horizontal components of surrounding rock pressure are indicated as Eqs. (3) and (4):

$$q_v = (0.2 \sim 0.3)\gamma_R b, \tag{3}$$

$$q_h = (0.05 \sim 0.10)\gamma_R h. \tag{4}$$

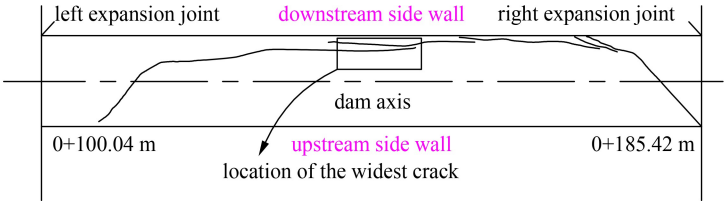

Fig. 5 Direction of corridor crack along dam axis.

The external water pressure exerted on the concrete lining is shown as follows:

$$P_e = \beta_e \gamma_w H_z, \tag{5}$$

where β_e is the reduction coefficient of external water pressure, γ_w is the bulk density of water, H_z is the elevation difference from water level to the center of corridor.

In the recent safety monitoring, it is found that there are many cracks on the downstream side wall of the corridor, leading to serious water seepage and even water spraying. It can be seen that the activity of seepage water has a severe impact on the stability of surrounding soil. Therefore, the value range of β_e is 0.65–1.00.

3.2 Linear elastic model

For the sake of simplifying the calculation and analyzing the deformation and stress state of the corridor preliminarily, the corridor concrete lining and concrete cut-off wall are considered as linear elastic model at first. Thus, only the elastic modulus and Poisson's ratio are necessary to be determined. The parameters of linear elastic model are shown in Table 1.

3.3 Mohr strength theory

Since the built-in corridor is mainly subjected to the pressure of the overlying dam body and the horizontal shear force of the water pressure, it is preliminarily judged that the corridor is in the compression-shear stress state [25]. The failure state of concrete can be estimated by Mohr strength theory. According to Mohr strength theory, the strength limit range of concrete can be determined by its tensile strength and compressive strength. The condition of shear damage is as:

$$\sigma_1 - \frac{\sigma_{bt}}{\sigma_{bc}}\sigma_3 > \sigma_{bt}, \tag{6}$$

where σ_1 and σ_3 are respectively the major and minor principal stresses, σ_{bt} and σ_{bc} are respectively the tensile and compressive strength of concrete.

Table 1 Parameters of linear elastic model

materials	γ (kN·m^{-3})	E (GPa)	v
new corridor lining	2400	30	0.167
original corridor lining	2400	24	0.167
concrete cut-off wall	2400	30	0.167

4 Analysis of corridor damage during actual dam construction

4.1 Dam construction and water storage process

In order to conform to the actual situation of dam construction and water storage, the load is divided according to the filling process and water storage height, and the incremental load is applied step by step. The process of dam construction and water storage is shown in Fig. 6. In each step of load increment, the average elastic constant corresponding to the average stress is used to linearize the nonlinear problem, and the midpoint increment method is utilized in the calculation of nonlinear finite element method to improve the iterative calculation accuracy.

As one of the most common nonlinear constitutive models describing the mechanical behavior of soil, Duncan−Chang model can well reflect the stress-strain relationship of soil and rockfill materials. Therefore, in this paper, the Duncan−Chang model was used for the materials of dam body and overburden [26]. The tangent modulus E_t and stress level S are expressed as

$$E_t = K p_a (\sigma_3 / p_a)^n (1 - R_f S)^2, \tag{7}$$

$$S = \frac{(\sigma_1 - \sigma_3)(1 - \sin\varphi)}{2c\cos\varphi + 2\sigma_3 \sin\varphi}, \tag{8}$$

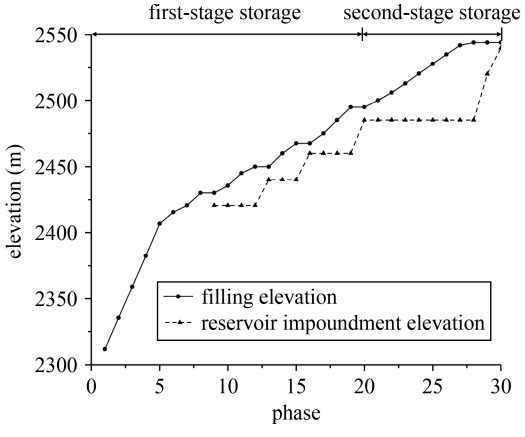

Fig. 6 Dam construction and water storage process.

with

$$\varphi = \varphi_0 - \Delta\varphi \lg(\sigma_3 / p_a). \tag{9}$$

where K is the modulus number, p_a is the atmosphere pressure, R_f is the failure ratio, c is the cohesive strength, φ is the internal friction angle, φ_0 is the initial internal friction angle, $\Delta\varphi$ is the increment of internal friction angle.

The bulk modulus K_t is expressed as follows:

$$K_t = K_b p_a \left(\frac{\sigma_3}{p_a}\right)^m. \tag{10}$$

where K_b is the bulk modulus number, n and m are exponents.

In case of unloading and reloading, if the deviatoric stress is less than the historical maximum deviatoric stress and the stress level is less than the historical maximum stress level, the elastic modulus E_{ur} is expressed as

$$E_{ur} = K_{ur} p_a \left(\frac{\sigma_3}{p_a}\right)^{n_{ur}}, \tag{11}$$

where K_{ur} is the modulus number under unloading and reloading condition, n_{ur} is the test parameter. Parameters of overburden and dam filling materials are shown in Table 2.

4.2 Nonlinear contact model

The deformation performance between concrete cut-off wall and overburden layer, and between concrete corridor lining and gravel soil core wall is of great difference, thus, staggered sliding and separation may occur along the contact interface under loads. In this paper, all contact surfaces are simulated by Goodman contact element [27,28].

Goodman contact element has only length but no thickness, and the contact surfaces are completely coincident initially. In the normal direction, a large stiffness modulus is generally adopted to prevent the overlap of the contact surface under pressure; in the tangential direction, the relationship between shear and shear deformation is described as nonlinear. Assuming that there is no interaction between the shear stresses in the two directions, the constitutive relationship of the contact surface is as

$$\begin{Bmatrix} \Delta\tau_1 \\ \Delta\tau_2 \end{Bmatrix} = \begin{bmatrix} k_{s1} & 0 \\ 0 & k_{s2} \end{bmatrix} \begin{Bmatrix} \Delta\gamma_1 \\ \Delta\gamma_2 \end{Bmatrix}, \tag{12}$$

where τ_1 and τ_2 are the shear stress in both directions of 2-D contact surface in 3-D model, respectively, γ_1 and γ_2 are the shear strain in two directions, k_{s1} and k_{s2} are tangent shear stiffness modulus, which can be expressed as follows:

$$k_{s1} = \left(1 - R_f \frac{\tau_1}{\sigma_n \tan\delta}\right)^2 K_1 \gamma_w \left(\frac{\sigma_n}{p_a}\right)^n, \tag{13}$$

$$k_{s2} = \left(1 - R_f \frac{\tau_2}{\sigma_n \tan\delta}\right)^2 K_2 \gamma_w \left(\frac{\sigma_n}{p_a}\right)^n, \tag{14}$$

where R_f is the shear failure ratio of contact surface, σ_n is the normal stress of contact surface, δ is the interface friction angle of contact surface; K_1, K_2, and n are nonlinear parameters determined by test, γ_w is the bulk density of water. According to Eqs. (13) and (14), the relationship between shear stress and relative shear displacement of contact surface conforms to hyperbola. Calculation parameters of contact surface are summarized in Table 3.

4.3 Concrete damaged plasticity model

The most notable characteristic of concrete material is the obvious mechanical difference between compressive and tensile behavior. The concrete damaged plasticity (CDP)

Table 2 Parameters of nonlinear constitutive relation of materials (Duncan-Chang E-v model)

materials	γ (kN·m^{-3})	K	n	c (kPa)	R_f	φ_0 (°)	G	D	F	K_{ur}	$\Delta\varphi$ (°)
rock-fill											
I	21.29	1000	0.35	0	0.79	48.5	0.43	4.5	0.25	2000	9.2
II	21.09	1200	0.35	0	0.83	50.0	0.40	4.0	0.20	2400	9.0
III	20.31	1000	0.28	0	0.82	51.5	0.38	5.4	0.19	2000	6.6
IV	20.04	1100	0.35	0	0.79	48.5	0.43	4.5	0.25	2200	9.2
core wall	22.34	494	0.4	66	0.82	28.9	0.43	2.8	0.09	988	0.0
contact clay	19.60	150	0.5	22	0.72	28.0	0.36	2.0	0.06	250	0.0
transition layer	20.58	990	0.15	0	0.82	54.1	0.38	2.4	0.22	1980	11.6
inverted filter layer	21.17	850	0.4	0	0.74	47.0	0.40	3.0	0.10	1700	8.5
overburden	23.82	600	0.5	30	0.76	30.0	0.35	3.5	0.03	1400	0.0

Table 3 Calculation parameters of contact surface

contact surface types	R_f	K_1	K_2	n	K_n	δ (°)
contact clay / corridor concrete	0.92	10000	10000	0.5	999000	20
overburden layer / corridor concrete	0.92	10000	10000	0.5	999000	20
overburden layer / cut-off wall concrete	0.92	8000	8000	0.5	999000	10
residual at the bottom of cut-off wall	0.6	15000	15000	0.5	50000	41

model defines the failure mechanism according to the tensile cracking and compressive crushing of materials. Based on the isotropic elastic damage theory and uncorrelated multiple hardening plasticity, CDP model is suitable for the simulation of irreversible damage of concrete [29–37].

4.3.1 Nonlinear behavior of concrete

The CDP model is based on the concepts of isotropic damage elasticity, isotropic tensile and compressive plasticity. Therefore, it is necessary to define the inelastic behavior of concrete at the beginning. In this study, the concrete constitutive relation given by Code for design of concrete structures (GB 50010-2010) is utilized to describe the compression and tension behavior of concrete [16]. The compressive stress-strain relationship is as follows:

$$\sigma = (1 - d_c) E_c \varepsilon, \tag{15}$$

where E_c is the elastic modulus of concrete, d_c is the compressive damage variable, which can be determined as Eq. (16):

$$d_c = \begin{cases} 1 - \dfrac{\rho_c n}{n - 1 + x^n}, & x \leqslant 1, \\ 1 - \dfrac{\rho_c}{\alpha_c (x-1)^2 + x}, & x > 1, \end{cases} \tag{16}$$

with

$$\rho_c = \frac{f_{c,r}}{E_c \varepsilon_{c,r}}, \tag{17}$$

$$n = \frac{E_c \varepsilon_{c,r}}{E_c \varepsilon_{c,r} - f_{c,r}}, \tag{18}$$

$$x = \frac{\varepsilon}{\varepsilon_{c,r}}, \tag{19}$$

where $f_{c,r}$ is the representative value of concrete uniaxial compressive strength, $\varepsilon_{c,r}$ is the ultimate compressive strain corresponding to uniaxial compressive strength $f_{c,r}$, α_c is the parameter of descending section of compression stress−strain curve for concrete.

The stress−strain curve of concrete compression is shown in Fig. 7.

The concrete tensile stress−strain relationship is expressed as Eq. (20):

$$\sigma = (1 - d_t) E_c \varepsilon, \tag{20}$$

$$d_t = \begin{cases} 1 - \rho_t \left(1.2 - 0.2 x^5\right), & x \leqslant 1, \\ 1 - \dfrac{\rho_t}{\alpha_t (x-1)^{1.7} + x}, & x > 1, \end{cases} \tag{21}$$

with

$$\rho_t = \frac{f_{t,r}}{E_c \varepsilon_{t,r}}, \tag{22}$$

$$x = \frac{\varepsilon}{\varepsilon_{t,r}}, \tag{23}$$

where $f_{t,r}$ is the representative value of concrete uniaxial tensile strength, $\varepsilon_{t,r}$ is the ultimate compressive strain corresponding to uniaxial tensile strength $f_{t,r}$, α_t is the parameter of descending section of tensile stress-strain curve for concrete.

Based on Eq. (20), the concrete tensile stress-strain curve can be obtained as illustrated in Fig.8.

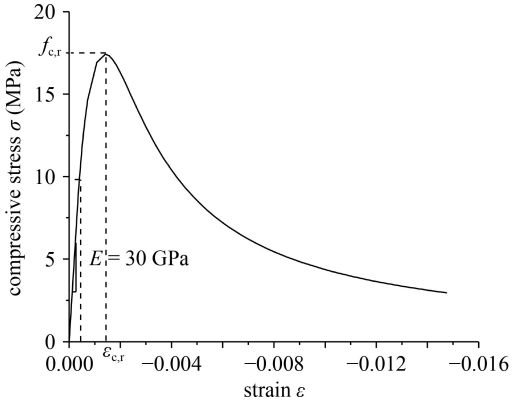

Fig. 7 Compression stress−strain curve for concrete.

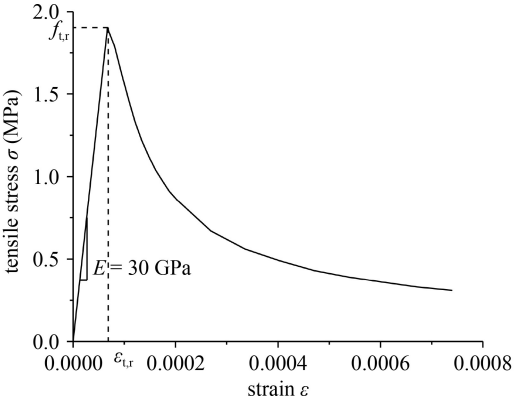

Fig. 8 Tension stress−strain curve for concrete.

4.3.2 Flow rule

The flow rule of CDP model is defined by assuming a non-associated potential plastic formula, which is as follows [38–40]:

$$\varepsilon^{\mathrm{pl}} = \lambda \frac{\partial G(\overline{\sigma})}{\partial \overline{\sigma}}, \tag{24}$$

where $\varepsilon^{\mathrm{pl}}$ is the plastic strain rate, λ is a non-negative multiplier, $\overline{\sigma}$ is the effective stress, G is the flow potential, which follows the Drucker−Prager hyperbolic function and can be defined as Eq. (25):

$$G = \sqrt{(\kappa \sigma_{\mathrm{t0}} \tan\psi)^2 + \overline{q}^2} - \overline{p}\tan\psi, \tag{25}$$

where κ is a parameter of eccentricity that defines the rate at which the function approaches the asymptote; σ_{t0} is the uniaxial tensile stress at failure; $\overline{p}$ and $\overline{q}$ are the hydrostatic stress and the von Mises equivalent effective stress, respectively; ψ is the dilation angle measured in the $p-q$ plane under high confining pressure.

4.3.3 Yield surface

The evolution of the yield surface is dominated by the hardening variables, $\varepsilon_{\mathrm{t}}^{\mathrm{pl}}$ and $\varepsilon_{\mathrm{c}}^{\mathrm{pl}}$. Generally, in terms of effective stresses, the yield function F is defined according to Eq. (26):

$$F = \frac{1}{1-\alpha}\left(\overline{q} - 3\alpha\overline{p} + \beta\left(\varepsilon^{\mathrm{pl}}\right)\left\langle\hat{\overline{\sigma}}_{\max}\right\rangle - \gamma\left\langle-\hat{\overline{\sigma}}_{\max}\right\rangle\right) - \overline{\sigma}_{\mathrm{c}}\left(\varepsilon_{\mathrm{c}}^{\mathrm{pl}}\right) = 0, \tag{26}$$

with

$$\alpha = \frac{(\sigma_{\mathrm{b0}}/\sigma_{\mathrm{c0}}) - 1}{2(\sigma_{\mathrm{b0}}/\sigma_{\mathrm{c0}}) - 1}, \qquad 0 \leqslant \alpha \leqslant 0.5, \tag{27}$$

$$\beta = \frac{\overline{\sigma}_{\mathrm{c}}\left(\varepsilon_{\mathrm{c}}^{\mathrm{pl}}\right)}{\overline{\sigma}_{\mathrm{t}}\left(\varepsilon_{\mathrm{t}}^{\mathrm{pl}}\right)}(1-\alpha) - (1+\alpha), \tag{28}$$

$$\gamma = \frac{3(1-K_{\mathrm{c}})}{2K_{\mathrm{c}} - 1}, \tag{29}$$

where $\hat{\overline{\sigma}}_{\max}$ is the maximum principal effective stress, K_{c} is the ratio of the tensile meridian to the compressive meridian, which is able to determine the shape of the yield surface, $\sigma_{\mathrm{b0}}/\sigma_{\mathrm{c0}}$ is the ratio of the initial equibiaxial compressive yield stress to the initial uniaxial compressive yield stress, $\overline{\sigma}_{\mathrm{c}}\left(\varepsilon_{\mathrm{c}}^{\mathrm{pl}}\right)$ and $\overline{\sigma}_{\mathrm{t}}\left(\varepsilon_{\mathrm{t}}^{\mathrm{pl}}\right)$ are the effective compressive and tensile cohesion stress, respectively [41,42].

The typical yield surface under the deviatoric and plane-stress conditions is shown in Fig.9. The intercepting points of the yield line on the principal stress axis specify the uniaxial tensile and compressive capacities. The tension decrease and the compression increase under biaxial stress conditions are shown in the graph.

Based on concrete biaxial and triaxial tests and engineering experience, parameters of the yield surface and flow rule of CDP model for concrete are obtained [43,44], and they are summarized in Table 4.

5 Damage analysis of built-in corridor

5.1 The finite element model

To analyze the stress state of the built-in corridor, estimate the reliability of various surrounding pressure calculation formulas, and explore reasonable design method for the built-in corridors, three schemes shown in Table 5 were considered for structural calculation of the corridor.

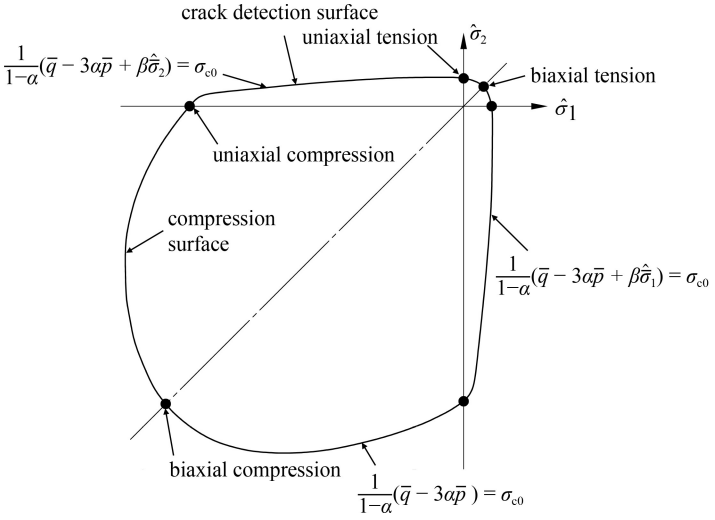

Fig. 9 Yield surface of the CDP in plane stress.

Firstly, the stress state of the foundation grouting corridor was analyzed based on the calculation formula of surrounding rock pressure, and Fig. 10(a) shows the local 3D finite element mesh of the corridor, with 19140 elements and 21861 nodes in it. The surrounding rock pressure applied on the corridor lining was calculated by Terzaghi formula and empirical formula in the specification for design of hydraulic tunnel (SL279-2012), respectively. The external water pressure was also calculated by the specification for design of hydraulic tunnel, which corresponds to the normal storage level situation. The bottom, front and rear surfaces of the model were set as fixed constraints. Since there are joint grouting and dowel bars carried out at the binding site between old and new concrete linings to reinforce their connection, it is considered that they will not be separated under stress. Therefore, the two layers of concrete linings can be regarded as one part.

For the sake of considering the influence of self-wight and structure of the dam on corridor, a quasi-three-

Table 4 The CDP model parameters for concrete

parameter	value
dilation angle	30
eccentricity	0.1
σ_{b0}/σ_{c0}	1.16
K_c	0.667
viscosity parameter	1.0×10^{-5}

Table 5 Calculation schemes of corridor structure analysis

calculation schemes	constitutive model of concrete	analysis method of corridor loads
scheme 1	linear elasticity	calculation formula of surrounding pressure, etc.
scheme 2	linear elasticity	considering actual dam construction
scheme 3	CDP	considering actual dam construction

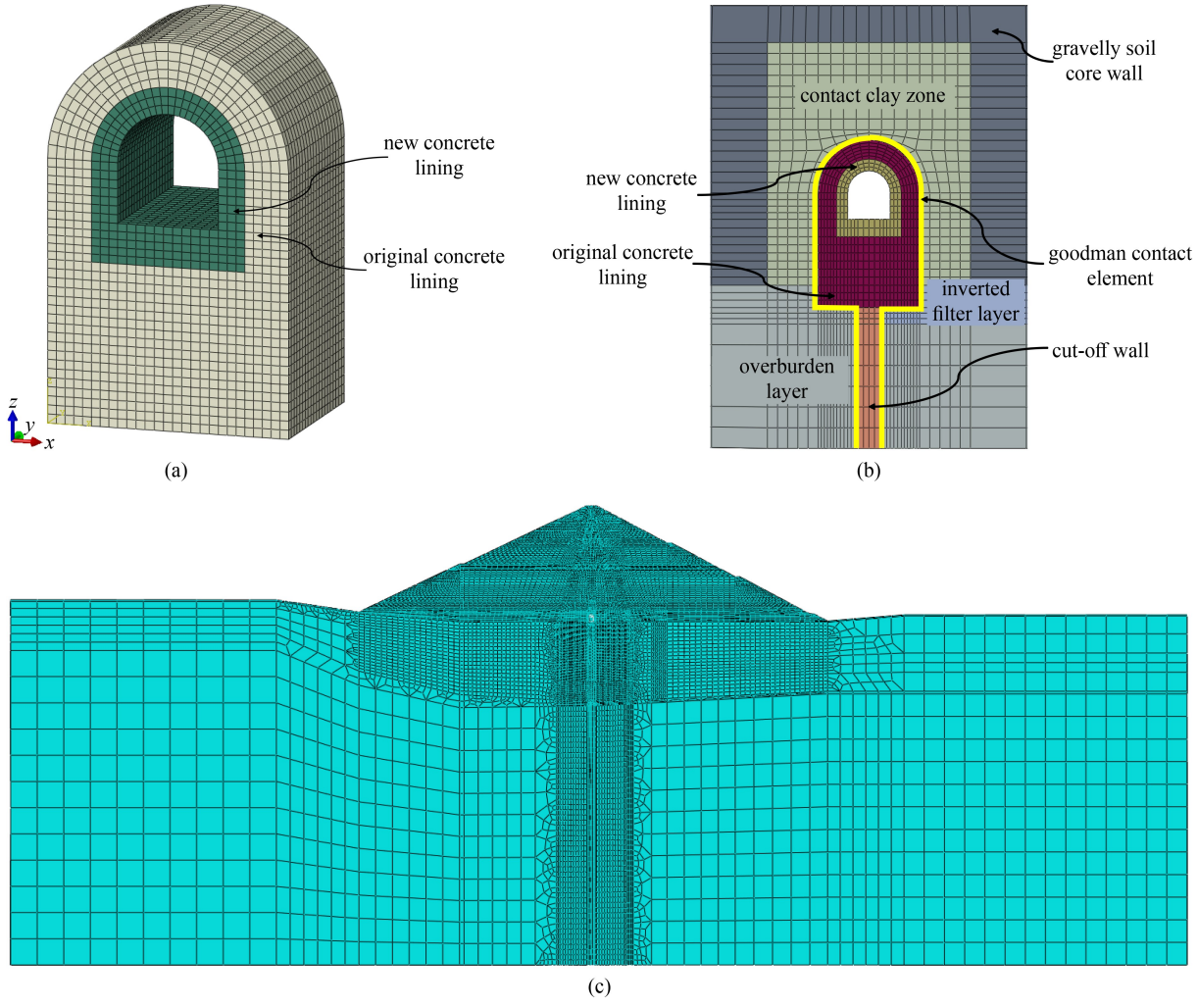

Fig. 10 3D finite element mesh of the dam model. (a) Local model of the corridor; (b) detail view of corridor area; (c) the global model.

dimensional (3D) finite element model of the global dam was established. The intersection of dam axis, the 0+150 m cross-section and 2000.00 m elevation line is taken as the origin of the model coordinate system, where the *X*-axis is along the river direction, the *Y*-axis is along the dam axis direction, and the *Z*-axis is vertically upward with the real elevation as its coordinates. The model boundaries in the upstream and downstream directions are respectively 656.00 and 672.00 m away from the dam axis. Figure 10(b) shows the detail view of the corridor area. Figure 10(c) displays the 3D finite element model with 60240 elements and 77570 nodes in it. The elements were divided into four layers along the thickness direction of the model, and the grid transition technology was utilized to locally densify the elements of corridor and cut-off wall.

According to the calculation parameters of core rockfill dam shown in Table 2, the nonlinear static finite element calculation was conducted. Firstly, the bedrock mass was loaded, and the overburden was loaded step by step, including the cut-off wall and contact surfaces. Then the dam body was loaded by stages, meanwhile, the built-in corridor, the contact surfaces, and the hydrostatic pressure were also loaded by stages according to the actual construction and water storage process illustrated in Fig. 1. Before loading the dam, the node displacement was initialized to zero and only the element stress was retained, so as to obtain the initial stress field of the foundation. Therefore, the displacements described below are only caused by the dam loading and water storage after foundation clearing. The displacement is positive in the direction along the coordinate axis, otherwise it is negative, with the unit of mm. The tensile stress is positive and the compressive stress is negative, with the unit of kPa.

5.2 Displacement of the built-in corridor

Summarize the displacement of each node on the corridor, and the contours of displacement distribution can be obtained, as shown in Fig. 11, where the coordinate $X = 0$ is the corridor centerline.

It is thus clear that the settlement of the downstream side of the corridor baseplate is larger than that of the upstream side. The corridor presents the phenomenon of downstream displacement, and the included angle between the baseplate and the horizontal plane is about 2.42°. The safety inspection data indicate that the corridor baseplate has an inclination towards the downstream at present, so the calculation results basically accord with the reality.

The relative displacement of contact surface elements between the corridor and the contact clay are able to determine whether they are separated. The relative displacement is positive for separation and negative for compression. According to the results shown in Fig. 12, except that the relative displacement of the contact elements at the corridor vault is small, the relative displacement of other regions is large. There are separations between the corridor baseplate and the overburden, and between the downstream side wall and the contact clay. Among them, the separation on the upstream side of the corridor baseplate is the most obvious.

5.3 Corridor stress and damage

5.3.1 Calculation results of scheme 1

In the case of scheme 1, the finite element static

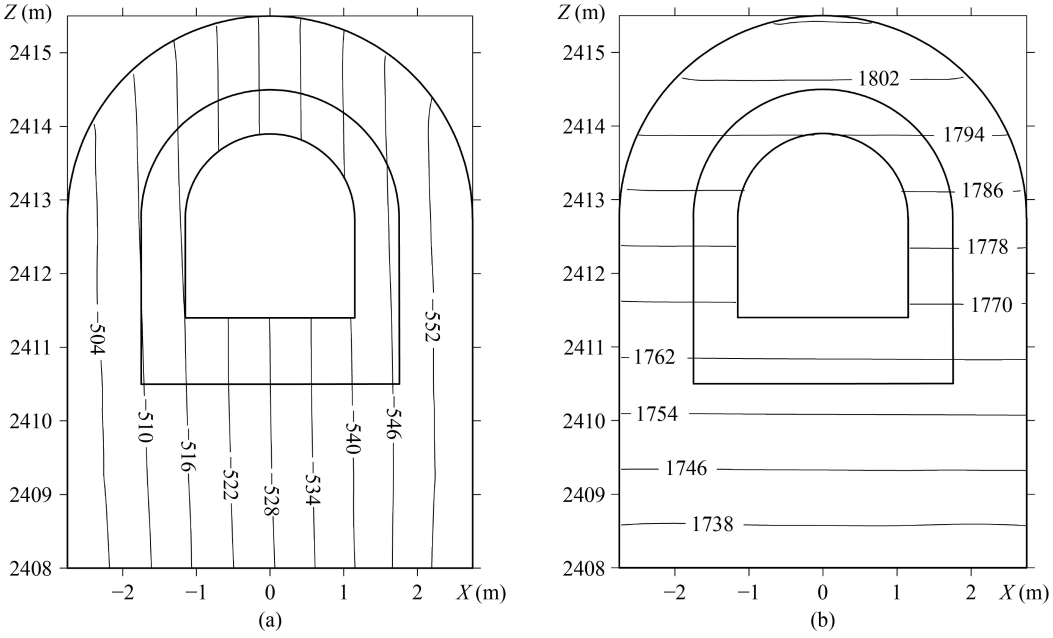

Fig. 11 Contours of corridor displacement: (a) settlement; (b) displacement along the stream direction.

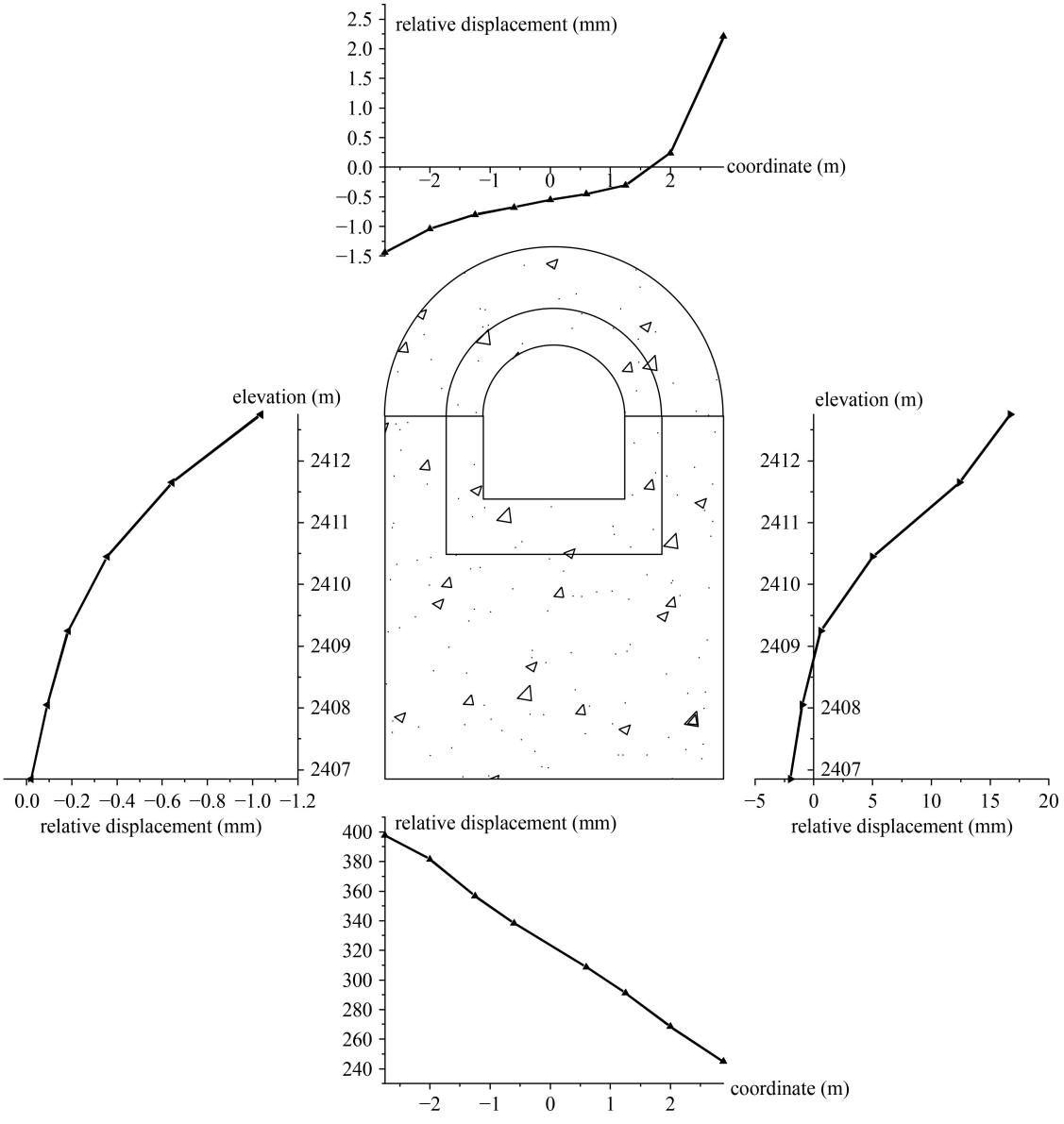

Fig. 12 The relative displacement of contact face elements around the corridor.

calculation was completed based on the built-in corridor local model shown in Fig. 10(a). The stress contours of the corridor baseplate and lining calculated by Terzaghi formula and empirical formula in the specification were respectively drawn, as shown in Figs. 13 and 14.

5.3.2 Calculation results of scheme 2

Under the condition of scheme 2, the calculation of corridor stress after dam filling and water storage is completed based on the model shown in Fig. 10(c). The contours of corridor stress are shown in Fig. 15.

It can be seen from Fig. 15 that the stress value at the downstream side wall of the corridor is obviously larger than other parts, which is called as the stress concentration phenomenon. Therefore, damage may occur at this location. Select three elements located on the downstream side wall of the corridor, and the locations of three elements are shown in Fig.16. The normal stresses in each direction and the 1st and 3rd principal stress are summarized in Table 6 (λ is the intersection angle between the 3rd principal stress plane and the horizontal plane).

In practical terms, the strength envelope of the material can be determined according to its tensile strength σ_{bt} and compressive strength σ_{bc}. Then the stress circle of an element was drawn by its principal stresses, and whether compression shear failure occurs at this element are able to be estimated through the relative position between the stress circle and the envelope.

According to the theory of material mechanics, under the action of 3-D stress, the development direction of element crack is generally parallel to the direction of the first principal stress surface (the tensile stress is positive

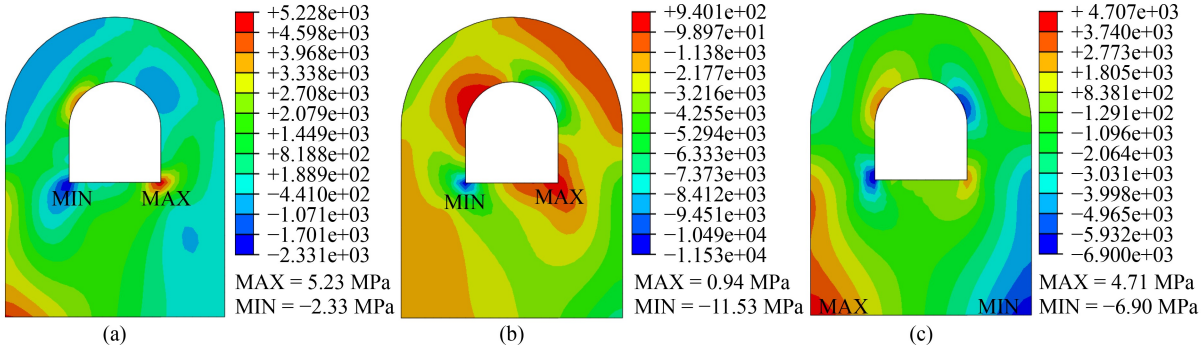

Fig. 13 Contours of corridor stress in scheme 1 based on Terzaghi formula. (a) 1st principal stress; (b) 3rd principal stress; (c) vertical normal stress.

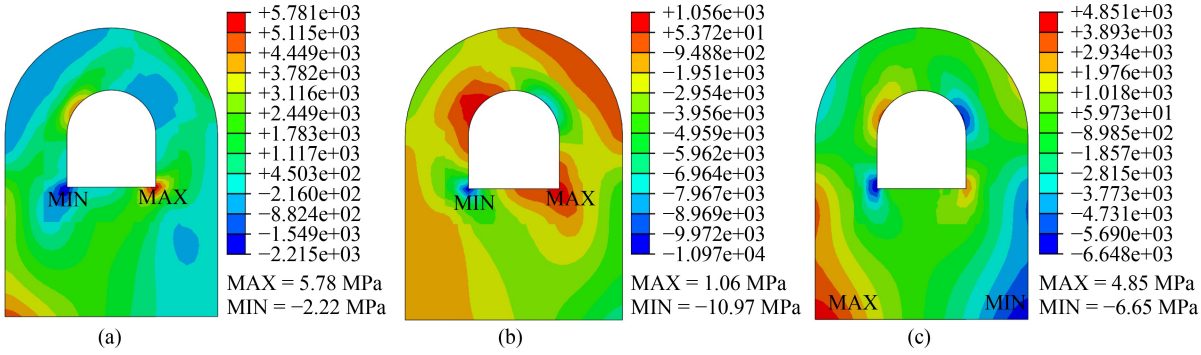

Fig. 14 Contours of corridor stress in scheme 1 based on specification. (a) 1st principal stress; (b) 3rd principal stress; (c) vertical normal stress.

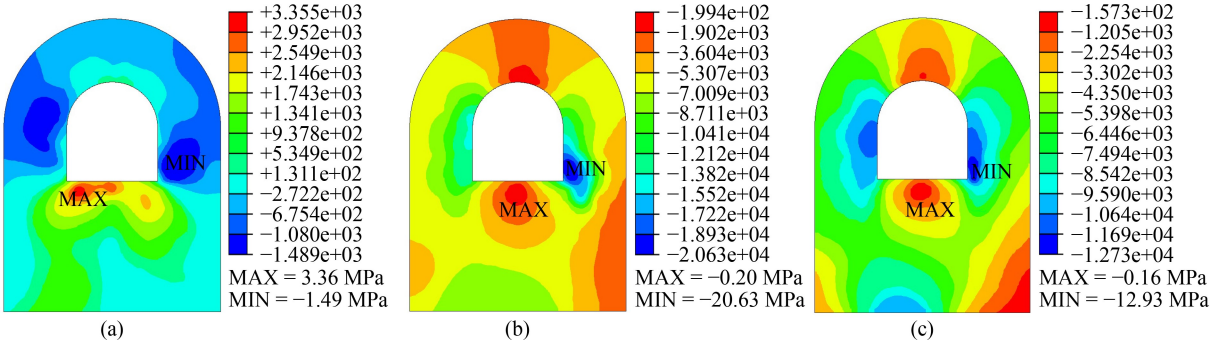

Fig. 15 Contours of corridor stress in scheme 2. (a) 1st principal stress; (b) 3rd principal stress; (c) vertical normal stress.

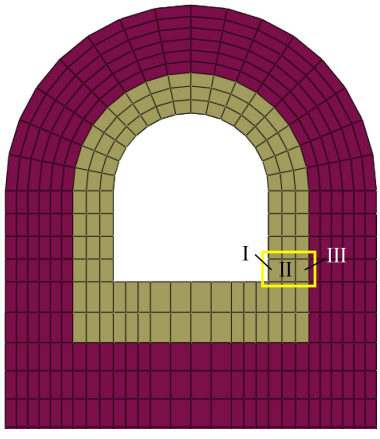

Fig. 16 Location illustrations of elements on the downstream side wall.

and the compressive stress is negative). The stress circle and estimated crack development direction of element I are illustrated in Fig. 17.

As is shown in Fig.17, the stress circle of element I have exceeded the strength envelope. For the same reason, the stress of element II and III are also beyond the ultimate stress. So it can be determined that the downstream side wall has been damaged, and the crack development direction (aka 1st principal stress direction) of each element is consistent with the actual cracking situation as shown in Fig. 2.

5.3.3 Calculation results of scheme 3

In scheme 2, the constitutive model of concrete was based on linear elastic model, so the stress in some regions of

the built-in corridor is too large. In fact, the local stress will be reduced after the concrete enters the plastic state or is damaged. Therefore, the previous analysis of corridor stress can only be used to deduce concrete cracking or compression shear failure. In order to calculate more accurately, the CDP model was used to analyze the stress of corridor combined with the actual construction process. The corridor stress calculation results in scheme 3 are shown in Fig. 18.

Table 6 Stress of elements on the downstream side wall

number	σ_{xx}	σ_{zz}	σ_{zx}	σ_1	σ_3	λ (°)
I	–803.81	–20077.24	3304.30	–253.05	–20628.00	9.5
II	–780.90	–17142.48	2467.20	–416.96	–17506.42	8.5
III	–582.32	–15649.19	1461.28	–441.90	–15789.61	5.7

The compressive damage variable d_c is adopted to indicate damage degree of concrete. When d_c is less than 0.1, the concrete is hardly damaged, when d_c is greater than 0.8, it implies that the concrete is seriously damaged. The compressive damage of corridor after dam filling and water storage is shown in Fig. 19.

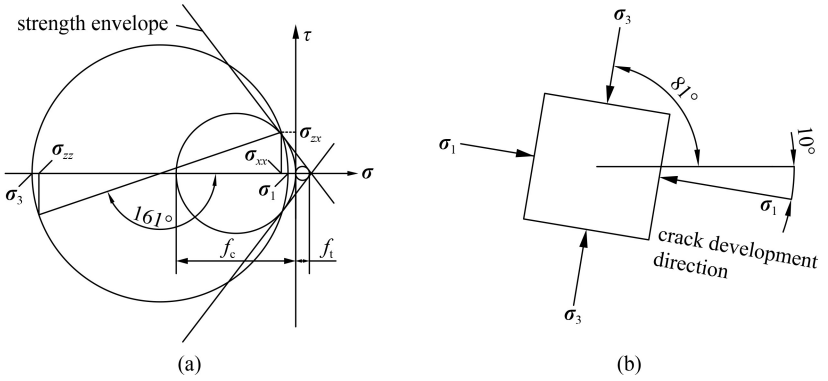

Fig. 17 The stress circle and crack development direction of element I. (a) The stress circle and strength envelope; (b) crack development direction.

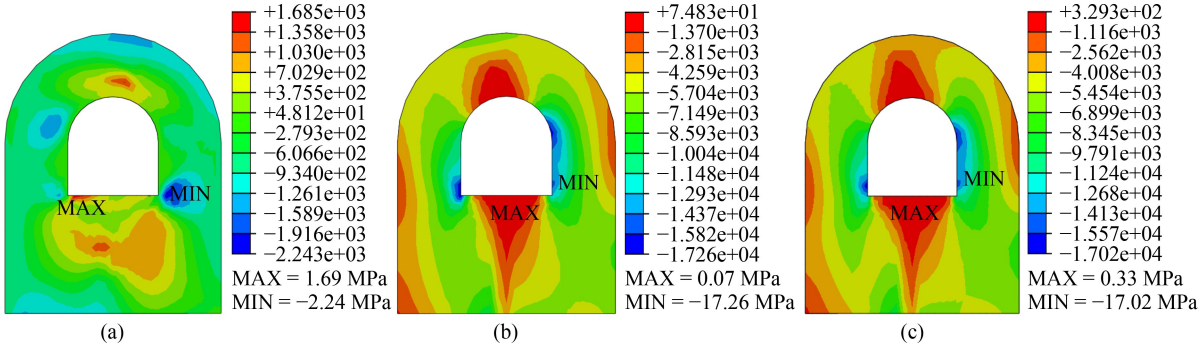

Fig. 18 Contours of corridor stress in scheme 3. (a) 1st principal stress; (b) 3rd principal stress; (c) vertical normal stress.

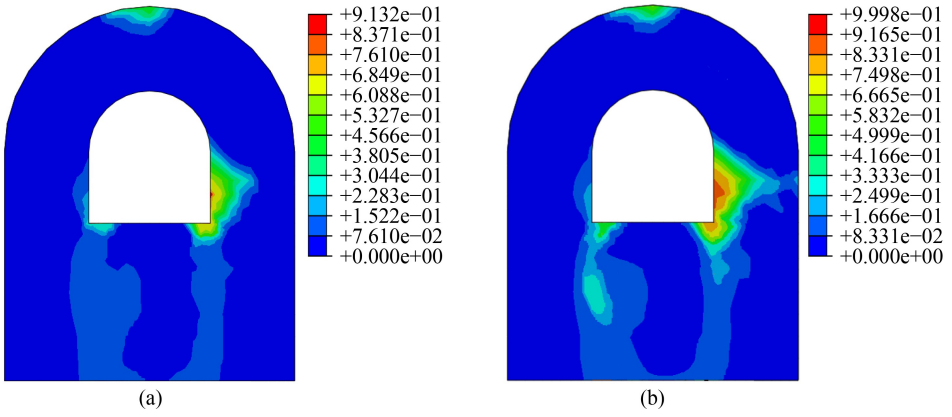

Fig. 19 Compressive damage of the built-in corridor. (a) After the completion of dam filling; (b) after the reservoir was filled to the normal water level.

In Fig. 19, it is clearly that the compressive damage of corridor mainly occurs in the downstream side wall, and the damage range gradually expands to the downstream side during the process of water storage, which conforms to the actual cracking phenomenon.

5.4 Results comparisons

5.4.1 Comparison between scheme 1 and scheme 2

The stress extremes of the built-in corridor obtained from three schemes are summarized and shown in Table 7. The concrete was regarded as linear elastic model in scheme 1 and scheme 2 to compare the rationality of different corridor load analysis methods. The surrounding rock pressure obtained by Terzaghi formula is greater than that obtained by empirical formula in specification for design of hydraulic tunnel. According to Table 7, under the condition of equal water pressure, the greater the surrounding rock pressure, the greater the maximum compressive stress and the smaller the maximum tensile stress.

The tensile and compressive stress obtained by scheme 1 are respectively higher and lower compared to scheme 2, which implies the surrounding soil pressure obtained by calculation formula is far less than the actual vertical earth pressure exerted on the built-in corridor. Therefore, for the built-in corridor of core rock-fill dam on thick overburden, its surrounding pressure cannot be calculated by general empirical formula, but needs to be specifically analyzed based on the actual construction situation of the dam and the structural characteristics of the corridor.

In addition, due to the different calculation models, there are also great differences in the corridor stress contour obtained in scheme 1 and scheme 2. The reasons for the differences are as follows: the bottom constraint of the corridor is not the fixed constraint shown in scheme 1 because of the separation between the overburden and the corridor baseplate; and in scheme 1 the water pressure is directly applied on the outside wall of the corridor in accordance with the normal storage level, without considering the anti-seepage effect of the core wall; last but not least, the frictional resistance caused by the relative displacement between contact clay, overburden and corridor is not taken into account. To sum up, the structural analysis of the corridor based on the surrounding pressure calculation and local model is not appropriate.

5.4.2 Comparison between scheme 2 and scheme 3

According to the calculation results of scheme 2, there is large compressive stress exerted on the downstream side wall of the built-in corridor, so the CDP model is used to further reveal the stress and damage behavior of the corridor in scheme 3. As shown in Figs. 15 and 18, the stress distribution and location of extreme value of the corridor are relatively similar, but there are great differences in the vault and baseplate in the case of the two schemes. Moreover, the extreme value of principal stress calculated by CDP model is significantly less than that calculated by linear elastic model. Furthermore, the calculation results of schemes 2 and 3 show that the compression damage of the corridor mainly occurs at the downstream side wall, but the results obtained by the linear elastic model can only be used to roughly evaluate the cracking state, and the calculation based on CDP model are able to reflect the compression damage distribution more intuitively, as shown in Fig. 19.

The extreme value of stress at each stage is collected and shown in Fig. 20. Before phase 20, the development trend of maximum stress based on the two constitutive models is relatively consistent. After phase 20, the maximum value of the 1st principal stress obtained in scheme 2 continues to increase, while the result of scheme 3 shows that the maximum value will be approximately stable to the uniaxial tensile strength of concrete. Similarly, unlike the continuous development of the minimum value of the 3rd principal stress in the case of linear elastic model, this value is nearly maintained at the uniaxial compressive strength after phase 22 under the condition of CDP model.

This phenomenon indicates that the extreme stress of the corridor has not reached the peak value of concrete strength before the dam was filled to 2500.00 m and the reservoir was stored to 2490.00 m. After that, with the subsequent construction and water storage, some areas of the corridor gradually enter the stage of compression or tensile damage. At this time, the distribution of stress will be locally adjusted according to the plastic behavior of concrete. So it is known that the CDP model can illustrate the stiffness degradation and stress redistribution of concrete more accurately, and then better describe the

Table 7 Summary of the stress extremes of the built-in corridor (unit: MPa)

calculation schemes	1st principal stress		3rd principal stress		vertical normal stress	
	Max	Min	Max	Min	Max	Min
scheme 1						
Terzaghi formula	5.23	–2.23	0.94	–11.53	4.71	–6.90
empirical formula	5.78	–2.22	1.06	–10.97	4.85	–6.65
scheme 2	3.36	–1.49	–0.20	–20.63	–0.16	–12.93
scheme 3	1.69	–2.24	0.07	–17.26	0.33	–17.02

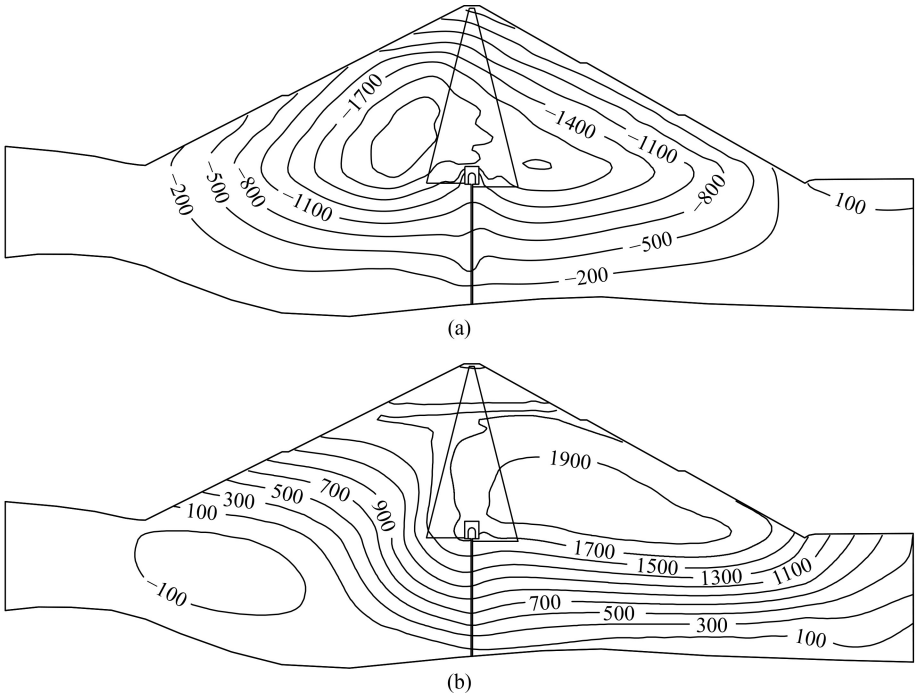

Fig. 20 Contours of displacement under normal storage level: (a) settlement; (b) displacement along the stream direction.

mechanical behavior of corridor damage compared with the linear elastic model.

At present, no cracking has been found in other areas of the corridor in the safety inspection, and the tensile stress area is small, as shown in Fig. 18. Besides, in the actual construction, the built-in corridor is reinforced by steel bars, which can effectively prevent the large-scale tensile cracking of the corridor side wall. Therefore, this paper mainly discusses the compression damage behavior of the corridor. In the future the role of reinforcement in the corridor can be investigated to study its influence on the stress and damage behavior of the corridor.

6 Discussion

6.1 Model rationality analysis and verification

For the sake of ensuring that the load imposed on the corridor in the numerical calculation conforms to the actual situation, the inverse analysis was firstly carried out according to the field settlement monitoring data of the downstream dam body. The material parameters of the dam were adjusted by finite element static calculation and Duncan−Chang model. After calculation, the displacement distribution of dam body under normal storage level is illustrated in Fig. 21. As shown in Fig. 21(a), the maximum settlement of the dam body appears in the upstream transition layer, with the value of 2470 mm, accounting for about 1.03% of the maximum dam height (including 95 m overburden); and the settlement of the core wall near the corridor is small. Thus, the dam settlement presents an uneven phenomenon of low in the middle and high on both sides. As shown in Fig. 21(b), both the dam crest and downstream slope present a trend of displacement to the downstream, with the maximum value of 1719 mm.

The stress distribution of dam body under normal storage level is shown in Fig. 22. The maximum stress of the dam body appears at the joint between the corridor and the bottom of the core wall, with the maximum 1st principal stress of 2.20 MPa and the maximum 3rd principal stress of 1.10 MPa. According to the stress distribution, there is stress concentration in the local area around the corridor.

As shown in Fig. 21, the calculation results of dam displacement are approximately consistent with the actual monitoring results illustrated in Fig. 3. In order to reflect the authenticity of the calculation results more intuitively, the comparison of monitoring and calculated values of the settlement at three different elevations on the downstream side of the dam body are summarized and shown in Fig. 23.

Besides, the location and development direction of corridor cracking also correspond to the actual situation, as shown in Fig. 2. Therefore, it is considered that both the FEM model and the calculation method are very reasonable. At the same time, the accuracy of the load borne by the built-in corridor has also been verified in this case.

6.2 Effect of thick overburden on rock-fill dam and its built-in corridor

In this study case, because the overburden is mainly composed of sand gravel and silty soil, the dam

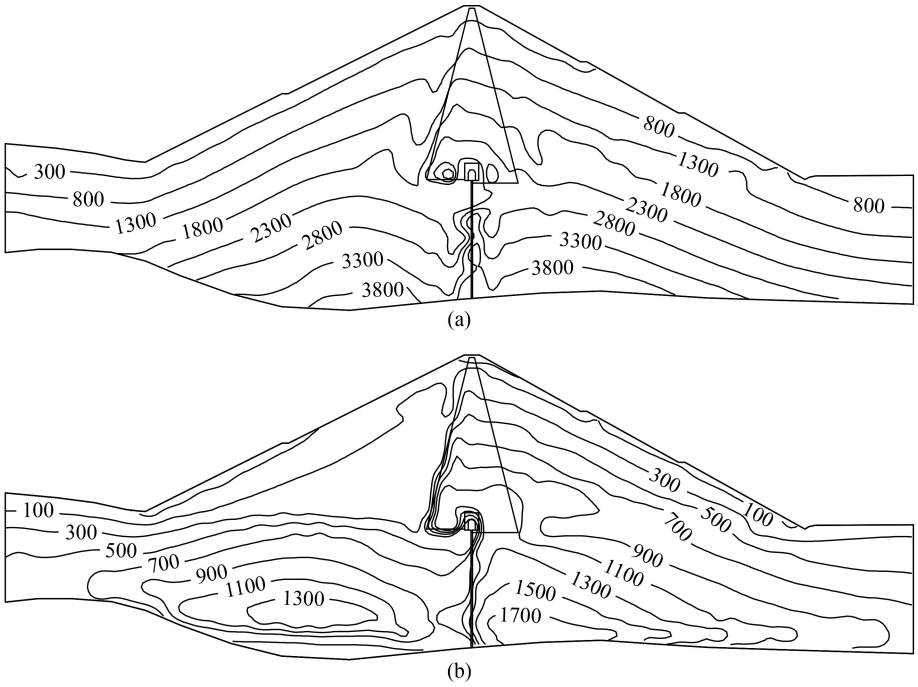

Fig. 21 Contours of stress under normal storage level. (a) 1st principal stress; (b) 3rd principal stress.

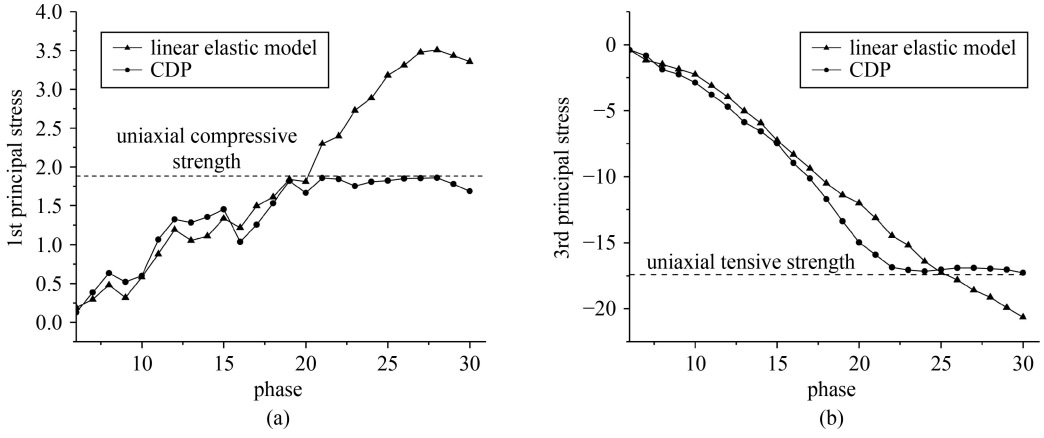

Fig. 22 Maximum value of corridor stress at each phase. (a) 1st principal stress; (b) 3rd principal stress.

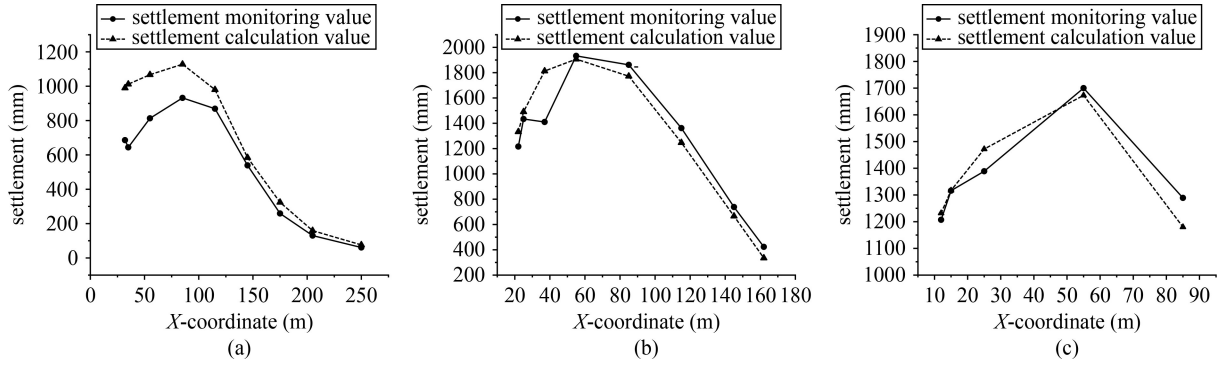

Fig. 23 Comparison of the monitoring values and calculated results of settlement at three different elevations on the downstream side of the dam. (a) 2420.00 m; (b) 2460.00 m; (c) 2500.00 m.

foundation material has the characteristics of high porosity, low strength and high permeability. Therefore, the concrete cut-off wall must be poured to a certain depth embedded in the bedrock to cut off the foundation

seepage. Meanwhile, since the thickness of the overburden is close to 100 m, the grouting amount is huge during the construction of the cut-off wall. Therefore, a grouting corridor must be set at the bottom of the core wall to ensure the convenience of construction and synchronization with the dam filling. As a result, the upstream of the cut-off wall and the bottom of the built-in corridor bear huge horizontal water pressure and uplift pressure, respectively.

On the other hand, the elastic modulus of the built-in corridor and cut-off wall made by concrete is much larger than that of the overburden. In this case, the settlement of the overburden was large under the weight of the dam and upstream water pressure, while the settlement of the corridor was small due to the supporting effect of the concrete cut-off wall and the lifting effect of uplift pressure. Additionally, because of the support of the cut-off wall and the built-in corridor, the settlement of the core wall at the dam axis is much smaller than that at the upstream and downstream sides of the dam. Therefore, the rock-fill dam presented the phenomenon of uneven settlement, as shown in Fig. 21(a). With the filling of the dam, because the compressibility of concrete cut-off wall is significantly lower than that of the overburden, the settlement difference between the overburden and the cut-off wall under the corridor baseplate was becoming larger and larger, resulting in the loss of support and eventual damage of the corridor.

In brief, the deformation difference between overburden and concrete under pressure is the fundamental reason for the abnormal deformation of rock-fill dam and the cracking damage of the built-in corridor.

6.3 Analysis on causes for damage of the corridor

As the result of the uneven settlement of dam foundation, the bottom of the built-in corridor separated from the overburden. Besides, the core wall and the corridor are compacted by the upstream water pressure and produce horizontal displacement toward downstream, as shown in Fig. 21(b). After separation from the overburden, the built-in corridor only had support at the connection between its bottom and the cut-off wall. Under the horizontal pressure of upstream water, the corridor tended to rotate around the top of the cut-off wall, which means the corridor baseplate tilted to the downstream side. Thus, the relative displacement of the corridor baseplate on the upstream side is greater than that on the downstream side. At the same time, the tilt of the corridor also led to the separation between the contact clay and the downstream side wall, as shown in Fig. 12.

The mechanical behavior of the built-in corridor mainly depends on the horizontal and vertical loads it bears. Assuming that the anti-seepage performance of the core wall is normal, the water pressure is exerted on the surfaces of the core wall. So the horizontal load on the corridor is mainly the lateral earth pressure on the side of the core wall transmitted by water pressure. With the rise of water level in the process of water storage, the lateral earth pressure difference on the upstream and downstream surfaces of the corridor is becoming larger and larger. The vertical loads borne by the corridor include the vertical earth pressure, the self-weight of the wall and the friction from the contact clay.

With the filling of the dam, because the compressibility of concrete is significantly lower than that of clay, there was an enormous settlement difference between the corridor and the contact clay under vertical loads. Then the settlement difference caused large friction on both sides of the corridor, and the friction direction is vertical and downward. Affected by the earth pressure and the vertical friction, the vertical stress of the side walls on both sides of the corridor is mainly compressive, as shown in Fig. 18(c).

With the rise of water level and the tilt of the corridor, the downstream side wall was gradually separated from the contact clay and lost its support. As a consequence, the downstream side wall presents a compression-shear state. On the other hand, the downstream side wall was in eccentric compression state and bent to the downstream side owing to the vertical pressure and friction. Thus, the outside compressive stress of the downstream side wall gradually decreased and changed into tensile stress. The inside compressive stress increased and caused compression damage, and the compression damage area gradually expands outward, as shown in Fig. 19.

7 Conclusions

Based on the dam safety inspection and numerical analysis, the damage behavior of built-in corridor in core rock-fill dam on thick overburden is analyzed in this paper. Two analysis methods based on the calculation of surrounding pressure and the actual dam construction process are considered. At the same time, the concrete constitutive model is also described as linear elastic model and CDP model, respectively. By comparing results of different calculation schemes, the damage causes of the corridor are discussed, and a reasonable corridor structure analysis method is put forward. According to the case study, the conclusions are as follows.

1) The damage of built-in corridor in earth rock dam is mainly determined by its upper load and structural characteristic. In this studied case, the upper load is mainly the self-weight of the dam body, and the uniqueness of the corridor structure is reflected in the different deformation performance of the overburden and the concrete cut-off wall. The composite action of the

self-weight of the dam and the uneven settlement of the foundation is the critical cause for the excessive compressive stress damage of the corridor.

2) The load of built-in corridor in earth rock dam on thick overburden cannot be estimated by conventional surrounding pressure calculation formula or empirical formula. The soil of the upper core wall of the corridor cannot form a stable collapse arch because of the uneven settlement, and the calculation results of conventional surrounding pressure are too small. And the mechanical behavior of the corridor can be described more reasonably by comprehensively considering dam filling, reservoir storage, contact between concrete and surrounding soil, and CDP model. The corridor load of such projects is related to factors including overburden thickness, mechanical properties of materials, dam height, and so on. The load shall be analyzed in combination with specific situations.

3) The elastoplastic model that can reflect plastic deformation and damage should be adopted for the numerical calculation of the built-in corridor. In this case, the CDP model can explain the stress redistribution and compression damage of concrete more reasonably compared with the linear elastic model.

4) Similar to the built-in corridor in earth rock dam, the traditional calculation formula for surrounding pressure is no longer applicable to tunnels with large buried depth, special geological conditions and complex structural forms in underground engineering. The calculation method used in this paper (scheme 3) may have good application value in the design and structure analysis of tunnels similar to built-in corridors.

Acknowledgements This work reported here was supported by the National Natural Science Foundation of China/Yalong River Joint Fund Project (Grant No. U1765205) and Jiangsu Colleges and Universities Advantageous Discipline Construction Project (Water Conservancy Project) (No. YS11001).

References

1. Fisk M. Late Quaternary Deltaic deposits of the Mississippi River (local sedimentation and basin tectonics). Geological Society of America, 1955, 62: 279−302
2. Liu S H, Wang L J, Wang Z J, Bauer E. Numerical stress-deformation analysis of cut-off wall in clay-core rockfill dam on thick overburden. Water Science and Engineering, 2016, 9(3): 219−226
3. Ma H, Sui W, Ni J. Environmentally sustainable mining: A case study on surface subsidence control of grouting into overburden. Environmental Earth Sciences, 2019, 78(10): 320
4. Akhenak A, Duviella E, Bako L, Lecoeuche S. Online fault diagnosis using recursive subspace identification: Application to a dam-gallery open channel system. Control Engineering Practice, 2013, 21(6): 797−806
5. Mirzabozorg H, Ghaemian M, Roohezamin A. The reason of cracking in bottom gallery of SefidRud Buttress Dam and earthquake and post earthquake performance. Structural Monitoring and Maintenance, 2019, 6(2): 103−124
6. Türkmen S. Water leakage from the power tunnel of Gezende Dam, southern Turkey: A case study. Environmental Earth Sciences, 2010, 61(2): 419−427
7. Zhang W G, Liu F, Jiao L C. Analyze and evaluation of deformation of structural joint and leakage at Qiaoqi Dam's foundation gallery. Modern Rockfill Dams, 2009: 767−773
8. Goel R K, Jethwa J L, Paithankar A G. Tunnelling through the young Himalayas—A case history of the Maneri-Uttarkashi power tunnel. Engineering Geology, 1995, 39(1−2): 31−44
9. Jeong S S, Han Y C, Kim Y M, Kim D H. Evaluation of the NATM tunnel load on concrete lining using the ground lining interaction model. KSCE Journal of Civil Engineering, 2014, 18(2): 672−682
10. Jiang Y, Yoneda H, Tanabashi Y. Theoretical estimation of loosening pressure on tunnels in soft rocks. Tunnelling and Underground Space Technology, 2001, 16(2): 99−105
11. Kim H J. Estimation for tunnel lining loads. Dissertation for the Doctoral Degree. Edmonton: University of Alberta, 1997
12. Zheng Y, Qiu C. On the Limitations of Protodyakonov's Pressure Arch Theory. Modern Tunnelling Technology, 2016, 53(2): 1−8
13. Zou H, Wei X, Sun Y. Study on difference of Chinese and foreign structural analysis method of tunnel lining. Yangtze River, 2016, 47(6): 48−64 (in Chinese)
14. SL279-2002. Water Conservancy Industry Standard of the People's Republic of China. Specification for Design of Hydraulic Tunnel. Beijing: China Water Power Press, 2003 (in Chinese)
15. TB10003-2016. Industrial Standards of the People's Republic of China. Code for Design of Railway Tunnel. Beijing: China Railway Press, 2017 (in Chinese)
16. GB 50010-2010. Code for Design of Concrete Structures. Beijing: China Architecture & Building Press, 2015 (in Chinese)
17. Häussler-Combe U, Hartig J. Formulation and numerical implementation of a constitutive law for concrete with strain-based damage and plasticity. International Journal of Non-linear Mechanics, 2008, 43(5): 399−415
18. Chiaia B, Fantilli A P, Vallini P. Combining fiber-reinforced concrete with traditional reinforcement in tunnel linings. Engineering Structures, 2009, 31(7): 1600−1606
19. Lee S Y, Lee S H O, Shin D I K, Son Y K, Han C S. Development of an inspection system for cracks in a concrete tunnel lining. Canadian Journal of Civil Engineering, 2007, 34(8): 966−975
20. Wang T T. Characterizing crack patterns on tunnel linings associated with shear deformation induced by instability of neighboring slopes. Engineering Geology, 2010, 115(1-2): 80−95
21. Nehdi M L, Abbas S. Exploratory study of ultra-high performance fiber reinforced concrete tunnel lining segments with varying steel fiber lengths and dosages. Engineering Structures, 2015, 101: 733−742
22. Yu T, Zhu A, Chen Y. Efficient crack detection method for tunnel lining surface cracks based on infrared images. Journal of Computing in Civil Engineering, 2017, 31(3): 04016067
23. Manuello A, Niccolini G, Carpinteri A. AE monitoring of a

concrete arch road tunnel: Damage evolution and localization. Engineering Fracture Mechanics, 2019, 210: 279−287
24. Mikkelsen L P, Klitgaard S J, Niordson C F, Sørensen B F. Tunneling cracks in arbitrary oriented off-axis lamina. International Journal of Fracture, 2020, 226(2): 161−179
25. Gu J, Chen P. A failure criterion for isotropic materials based on Mohr's failure plane theory. Mechanics Research Communications, 2018, 87: 1−6
26. Duncan J M, Chang C Y. Nonlinear analysis of stress and strain in soils. Journal of the Soil Mechanics and Foundations Division, 1970, 96(5): 1629−1653
27. Goodman R E, Taylor R L, Brekke T L. A model for the mechanics of jointed rock. Journal of the Soil Mechanics and Foundations Division, 1968, 94(3): 637−659
28. Huang D, Tang A, Wang Z. Analysis of pipe-soil interactions using goodman contact element under seismic action. Soil Dynamics and Earthquake Engineering, 2020, 139(5): 106290
29. Pedersen R R, Simone A, Sluys L J. An analysis of dynamic fracture in concrete with a continuum visco-elastic visco-plastic damage model. Engineering Fracture Mechanics, 2008, 75(13): 3782−3805
30. Yu T, Teng J G, Wong Y L, Dong S L. Finite element modeling of confined concrete-II: Plastic-damage model. Steel Construction, 2010, 32(3): 680−691
31. Abu Al-Rub R, Kim S M. Computational applications of a coupled plasticity-damage constitutive model for simulating plain concrete fracture. Engineering Fracture Mechanics, 2010, 77(10): 1577−1603
32. Jukic M, Brank B, Ibrahimbegovic A. Failure analysis of reinforced concrete frames by beam finite element that combines damage, plasticity and embedded discontinuity. Engineering Structures, 2014: 75: 507–527
33. Yan J B, Qian X, Liew J, Zong L. Damage plasticity based numerical analysis on steel–concrete–steel sandwich shells used in the Arctic offshore structure. Engineering Structures, 2016, 117: 542−559
34. Othman H, Marzouk H. Applicability of damage plasticity constitutive model for ultra-high performance fibre-reinforced concrete under impact loads. International Journal of Impact Engineering, 2018, 114: 20−31
35. Kenawy M, Kunnath S, Kolwankar S, Kanvinde A. Concrete uniaxial nonlocal damage-plasticity model for simulating post-peak response of reinforced concrete beam−columns under cyclic loading. Journal of structural engineering, 2020, 146(5): 04020052
36. Seok S, Haikal G, Ramirez J A, Lowes L N, Lim J. Finite element simulation of bond-zone behavior of pullout test of reinforcement embedded in concrete using concrete damage-plasticity model 2 (CDPM2). Engineering Structures, 2020, 221: 110984
37. Lj A, Mao A, Jian J B, Au A. Modelling concrete slabs subjected to fires using nonlinear layered shell elements and concrete damage-plasticity material. Engineering Structures, 2021, 234: 111977
38. Nechnech W, Meftah F, Reynouard J M. An elasto-plastic damage model for plain concrete subjected to high temperatures. Engineering Structures, 2002, 24(5): 597−611
39. Krätzig W B, Pölling R. An elasto-plastic damage model for reinforced concrete with minimum number of material parameters. Computers & Structures, 2004, 82(15−16): 1201−1215
40. Feng DC, Wu G, Sun Z Y, Xu J G. A flexure-shear Timoshenko fiber beam element based on softened damage-plasticity model. Engineering Structures, 2017, 140: 483−497
41. Yu T, Teng J G, Wong Y L, Dong S L. Finite element modeling of confined concrete-I: Drucker−Prager type plasticity model. Engineering Structures, 2010, 32(3): 665−679
42. Jiang J F, Wu Y F. Identification of material parameters for Drucker−Prager plasticity model for FRP confined circular concrete columns. International Journal of Solids and Structures, 2012, 49(3-4): 445−456
43. Lubliner J, Oliver J, Oller S, Onate E. A plastic-damage model for concrete. International Journal of Solids and Structures, 1989, 25(3): 299−326
44. Genikomsou A S, Polak M A. Finite element analysis of punching shear of concrete slabs using damaged plasticity model in ABAQUS. Engineering Structures, 2015, 98: 38−48